Biochemistry

pubs.acs.org/biochemistry Article

Intermolecular and Intramolecular Interactions of the *Arabidopsis* Plasma Membrane Proton Pump Revealed Using a Mass Spectrometry Cleavable Cross-Linker

Thao T. Nguyen, Matthew R. Blackburn, and Michael R. Sussman*

Cite This: *Biochemistry* 2020, 59, 2210–2225 Read Online

ACCESS | Metrics & More | Article Recommendations | Supporting Information

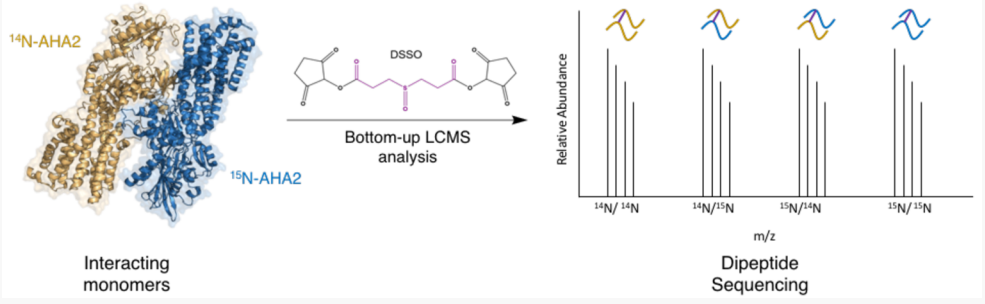

ABSTRACT: In plants and fungi, the plasma membrane proton pump (H^+-ATPase) establishes an electrochemical gradient across the plasma membrane, which serves as the driving force for the secondary transport of ions and nutrients across the cell membrane. This is an essential enzyme that functions in many important processes including stomatal movement, cell elongation, and cellular responses to stimuli from hormones, light, and other environmental conditions. Therefore, understanding how the activity of the H^+-ATPase is regulated is important to understand how plants adapt to different growth conditions. The autoinhibitory effect of the C-terminal regulatory domain of H^+-ATPase is well-established and is thought to be mediated by interactions with the catalytic domains. Here, using the lysine reactive mass spectrometry cleavable cross-linker DSSO, we found that the C-terminal domain of the *Arabidopsis* H^+-ATPase 2 (AHA2) cross-linked extensively with the actuator, nucleotide-binding, and phosphorylation domains, suggesting that the C-terminal domain regulates the catalytic cycle by modulating the relative positions of these domains. Interestingly, several C-terminal cross-links occurred near a predicted proton binding site (Asp-684 in TM6), suggesting that the C-terminal domain may regulate proton efflux. Additionally, cross-links between the C-terminal domain and other domains of AHA2 were detected in a monomeric protein resolved on SDS-PAGE, suggesting that intramolecular interactions may also be involved in the regulation of enzyme activity. Finally, we observed mixed-isotope cross-linking between the C-terminal domain and other domains of ^{14}N-AHA2 (unlabeled) and ^{15}N-AHA2 (labeled), supporting our model that oligomeric H^+-ATPase may autoinhibit the neighboring monomer in a "head-to-tail" configuration.

The H^+-ATPase is the primary energy transducing ion pump in the plasma membrane of yeast and plants and creates a proton motive force that energizes many other secondary transporters and channels.[1,2] In addition to its dominant role in cell surface energetics, this enzyme has multiple physiological functions in higher plants, including regulation of cell elongation and responses to abiotic and biotic stimuli like phototropic light and the plant hormones auxin and RALF (rapid alkalinizing factor).[3,4] The proton pump is a multipass, ~950 amino acid membrane protein containing 10 α-helical transmembrane domains, an apparently unstructured/disordered C-terminal regulatory domain, and three catalytic domains: the nucleotide-binding subdomain, the phosphorylation subdomain and the actuator subdomain.[5] The C-terminal domain consists of approximately the last 100 amino acids and is thought to autoinhibit enzyme activity by interacting with one or more portions of the rest of the enzyme.[1,2,6] This conclusion is based on early studies showing that removal of the C-terminal domain by either protease treatment or deletion mutagenesis activates the enzyme.[7−10] A specific mechanism has been invoked, which involves the regulation of the stoichiometry of protons ejected per ATP molecule hydrolyzed, although unlike other ATPases, there is no clear domain in the protein that is responsible for this important energetic coupling.[11,12] In addition, whether the C-

Received: April 3, 2020
Revised: May 26, 2020
Published: May 27, 2020

https://dx.doi.org/10.1021/acs.biochem.0c00268
Biochemistry 2020, 59, 2210–2225

terminal domain actually interacts with other domains as well as its 3D structure and binding location during inhibition of enzyme activity are important deficits in our understanding of how this enzyme operates. In a prior study, we used site-specific photo-cross-linking with the genetically encodable unnatural amino acid BPA to investigate the regulatory behavior of the C-terminal domain of *Arabidopsis* H^+-ATPase 2 (AHA2). In that work, we found the first direct evidence that the C-terminal domain interacts with the actuator domain of another monomer of AHA2 and therefore may regulate the enzyme activity in a "head-to-tail" monomer−monomer fashion.[13] However, the large size of the C-terminal domain (ca. 100 amino acids) suggests that this domain may interact with and regulate other regions of the enzyme. Thus, we sought additional methods to address this question.

Chemical cross-linking in combination with mass spectrometry (XL-MS) is a technically challenging, but powerful means of identifying protein−protein interactions at single residue resolution that can be performed in impure samples and requires only microgram amounts of protein. In this manner, it possesses a remarkable advantage over other structural methods such as NMR or X-ray crystallization, which rely on large (milligram) amounts of protein and require pure protein. Chemical cross-linkers connect specific pairs of amino acids, such as lysine−lysine, lysine−cysteine, cysteine−cysteine, or lysine−aspartate/glutamate residues. This cross-linking occurs within a given distance depending on the length of the cross-linker used, and thus these cross-linkers can act as a molecular "ruler" for predicting distances between amino acids in the 3D structure of a protein.[14−16] The data collected from XL-MS can be used to derive the geometrical constraints between these residues, supplementing missing information for disordered regions in pre-existing structures, and can even be useful for producing de novo protein structure models.[17,18] Furthermore, cross-link quantification can be used to reveal the conformational change of protein and protein complexes under different *in vitro* and *in vivo* conditions.[19−21]

The cross-linker DSSO (disuccinimidyl sulfoxide) links lysine to lysine and has a mass-spectrometry-labile sulfoxide bond within the 10.3 Å linker, which helps to identify cross-linking peptides with high confidence.[22] This sulfoxide bond is broken under the low energy collision-induced dissociation (CID) during MS/MS acquisition and results in two pairs of signature peaks with a unique mass difference of 31.97 Da in the MS2 spectrum, which significantly improves the confidence in identification of the cross-linked peptides. This cleavage step releases the two peptides from their cross-link, allowing them to be independently fragmented and sequenced with routine database searching algorithms. As a result, interpretation of the cross-linked spectrum is greatly simplified, and cross-links are identified with higher confidence compared to noncleavable cross-linkers. Recently, the Heck lab developed the software XlinkX for the identification of cross-links with gas-phase cleavable cross-linkers like DSSO. This has made data analysis much more straightforward and is especially powerful for studying proteome-wide protein interactions.[23,24] It is now possible to identify thousands of cross-links from *E. coli*, HeLa cell lysates, and mouse heart mitochondria, demonstrating the power of this technique.[23−25]

In this study, we used DSSO to further investigate the interaction between the C-terminal domain and other domains of AHA2. We also combined a $^{15}N/^{14}N$ AHA2 isotopologue mixing strategy with DSSO cross-linking to investigate intermolecular interactions in AHA2. The observation of $^{14}N/^{15}N$ and $^{15}N/^{14}N$ peaks from several cross-links between the C-terminal domain and other domains of AHA2 isotopologues support our hypothesis that the C-terminal domain may regulate the enzyme activity by interacting with other domains on nearby monomers in a "head-to-tail" fashion.[13] Additionally, these intermolecular cross-links between the domains implicate the intermonomer interfaces of oligomeric AHA2. Finally, cross-links between the C-terminal domain and other domains of AHA2 were also observed in the monomer cut from gel slices of the DSSO-cross-linked AHA2, suggesting that intramolecular interactions may also form a default mode of interaction in the absence of oligomerization. In both cases, the effect of each interaction depends on where the C-terminal domain interacts at any given time, and thus merits further study.

MATERIALS AND METHODS

Yeast Cell Culture and Protein Purification. Cells from the yeast strain RS72 were transformed with a vector containing strep-HA-tagged AHA2 (Uniprot accession number: P19456) under the yeast PMA1 promoter as described previously.[13] Yeast was grown in a selective medium for 2−3 days and subsequently transferred to a rich YPD medium to express AHA2. All of the following steps described below were performed at 4 °C. Cells were collected by centrifugation at 5000*g* and washed three times with ddH_2O. Cells were broken with a cell disrupter (PBI) for 2 passes at 35 kpsi in buffer A (20 mM HEPES, 150 mM KCl, 2 mM EDTA, 1.5 mM $MgCl_2$, and 0.5 mM ATP, pH 7.6, with freshly prepared protease cocktail inhibitor). Cell debris was removed by centrifugation at 5000*g* for 10 min in rotor SA-80. The supernatant was centrifuged at 33 000 rpm for 2 h to collect the microsomal fraction. The microsomal fraction was resuspended in buffer B (buffer A supplement with 10% glycerol, 1.5% DDM) and resolubilized for 3 h in a cold room. The insoluble fraction was sedimented by centrifugation at 33 000 rpm for 30 min and discarded. The supernatant was then diluted two times with buffer B without DDM and incubated with preequilibrated streptactin resin overnight at 4 °C on a rotator. The unbound material was eliminated by centrifugation at 1500 rpm for 5 min at 4 °C. The resin was then loaded to a column and washed with buffer C (20 mM HEPES, 150 mM KCl, 2 mM EDTA, 1.5 mM $MgCl_2$, and 0.5 mM ATP, pH 7.6, 0.05% DDM) then washed with buffer D (20 mM HEPES, 500 mM KCl, 2 mM EDTA, 1.5 mM $MgCl_2$, and 0.5 mM ATP, pH 7.6, and 0.05% DDM), and washed again with 20 resin volumes of buffer D. The strep-HA-tagged AHA2 was then eluted with 2.5 mM Desthiobiotin in buffer C with protease inhibitor cocktail. Protein eluates were then concentrated and exchanged into cross-linking buffer (20 mM HEPES, 150 mM KCl, 1.5 mM $MgCl_2$, 0.5 mM ATP, 0.05% DDM, pH 7.6) using 50 kDa MWC filter (MiliporeSigma).

Production of ^{14}N and ^{15}N AHA2. The DNA fragment containing strep-HA-tagged AHA2 was PCR-amplified with Pfu Ultra High-Fidelity DNA Polymerase (Agilent). The PCR products were then incubated with Taq polymerase (Takara) for another 15 min at 72 °C to add 3′ adenine overhangs. The strep-HA-tagged AHA2 fragment was then ligated into the pCR8 vector using the pCR8/GW/TOPO-TA cloning kit (Thermo Fisher Scientific), and strep-HA-tagged AHA2 was then transferred to the expression vector pAG423GAL-ccdB vector (Addgene) using the Gateway LR Clonase II enzyme

https://dx.doi.org/10.1021/acs.biochem.0c00268
Biochemistry 2020, 59, 2210−2225

mix (Thermo Fisher Scientific). The direction of the construct and sequence was then confirmed with DNA sequencing. The plasmid was then transformed into yeast strain T71 (MATα, *his3*Δ*1*) (courtesy of Dr. Michael Culbertson) and grown in selective medium YNB without any amino acids. Colonies from the plate were grown in liquid YNB containing ^{14}N ammonium sulfate or ^{15}N ammonium sulfate for 5 days with supplementing every day with glucose. Protein expression was induced by the addition of 2% galactose overnight at 30 °C. Equal amounts of yeast cells were mixed together, and all other steps for purifying AHA2 were performed, as described in the previous section.

Cross-Linking Reaction. Protein concentration was determined using the Bradford assay (Thermo Fisher Scientific). DSSO was then added to purified AHA2 at a molar ratio of 100:1, and the reaction mixture was incubated at room temperature for 1 h. The reaction was then quenched with the addition of 200 mM Tris buffer for 15 min at room temperature. The cross-linking reaction was then either digested in-solution directly, or resolved on a 4−12% SDS-PAGE gel (Invitrogen Bolt gel) first and then subjected to in-gel digestion. For isotope-assisted DSSO cross-linking, we lysed equal portions of cells based on an optical density of 600 nm and purified as described. We then preincubated the samples at 37 °C for 30 min before adding DSSO. The reaction proceeded for 1 h at room temperature until quenching as described.

Protein Digestion and Clean up. For in-solution digestion, protein samples were prepared in either of two ways: with on-column digestion using the S-trap method[26] (Protifi) according to the manufacturer's protocol (which utilizes SDS denaturation under acidic conditions), or by digestion following acetone precipitation as previously described.[27] Precipitated protein was then dissolved in 9.5 M urea and 50 mM ammonium bicarbonate. The samples were then reduced with 5 mM DTT (dithiothreitol) in 50 mM ammonium bicarbonate buffer for 1 h at 42 °C and alkylated with 15 mM IAA (iodoacetamide) in 50 mM ammonium bicarbonate for 30 min in the dark. All buffers and solutions described here were freshly prepared at the time of experimentation. The alkylation was stopped by adding another 5 mM DTT for 15 min at 37 °C. The samples were then diluted with 50 mM ammonium bicarbonate to ∼1 M urea and digested with LysC (Wako) at a 1:50 ratio for at least 3 h, followed by digestion with trypsin at ratio 1:40 overnight at 37 °C shaking at 200 rpm in an incubator. For double digestion, GluC or chymotrypsin was then added at a ratio of 1:100; the samples were then incubated at 37 °C for another 5−8 h. The digestion was stopped with the addition of TFA to a final concentration of 0.35% and spun down for 5 min on a tabletop centrifuge at 17 000 rcf. The supernatant was transferred to a new low-protein binding tube and cleaned with OMIX C18 tips (Agilent Technologies). The peptides were then eluted with 80% acetonitrile/0.1% TFA and dried in a vacuum. For the whole-cell extract of the ^{14}N mixed ^{15}N sample, the peptides were fractioned using high pH reversed-phase spin columns (Thermo Fisher Scientific). The peptides were redissolved in 0.1% formic acid (LC−MS grade, Fisher Scientific). For in-gel digestion, the protocol was as in the previous study.[13]

NanoLC−MS/MS. Peptide mixtures were separated on an Ultimate 3000 RSLC nanosystem with C18 column: Acclaim PepMap, 75 μm × 25 cm, 2 μm, 100 Å (Thermo Fisher Scientific). A gradient from 2% to 40% B was used with a flow rate of 300 nL/min (5−43 min gradient time). For the peptide sample digested in solution, a longer gradient elution from 5 to 100 min was used instead. The peptides were then further eluted for 5 min with 40% to 90% B. The column was then washed with 90% B for 5 min and re-equilibrated with 100% buffer A for 12 min. Solvent A: water + 0.1% formic acid. Solvent B: acetonitrile + 0.01% formic acid. The nano-HPLC system was directly coupled to an Orbitrap Fusion Tribrid mass spectrometer with an EASY spray Source (Thermo Fisher Scientific). Data were acquired in data-dependent MS/MS mode. Each high-resolution full scan (R = 60 000) in the orbitrap was followed by high-resolution product ion scans (R = 30 000) within 5 s, starting with the most intense signal in the full scan mass spectrum (isolation window of 2 m/z); the target value was set to 50 000, and maximum accumulation time was set to 200 ms. Dynamic exclusion (exclusion duration of 16 s exclusion window of ±10 ppm) was enabled to detect less abundant ions. Only precursors with charge states from 3+ to 8+ were selected for MS/MS. For CIDMS2-HCDMS2 acquisition, sequential fragmentation with CID at 25% normalized collision energy (NCE), and stepped HCD (30 ± 5% NCE) were used to obtain MS2 spectrum. For CIDMS2-HCDMS3 acquisition, CID fragmentation energy was set to 25% NCE, then the four most abundant reporter doublets from MS/MS scans (charge states 2−6, Δ mass 31.9721 Da, ± 30 ppm) were selected for MS3. MS3 scans were recorded in the ion trap operated in rapid mode with a maximum fill time of 150 ms (isolation width 2.0 m/z). Fragmentation was carried out using stepped HCD by applying a collision energy of 30 ± 5% NCE. For CID-MS2/ETD-MS2 or CID-MS2/EThcD-MS2, the methods were adapted from a previous study.[28]

Data Analysis. Acquired mass spectra raw files were analyzed using Thermo Scientific Proteome Discoverer 2.2 software using the XlinkX node. The target search database was the AHA2 sequence with other yeast proteins identified in the purified AHA2 sample supplemented with the sequences of common keratin contaminant proteins. Mass spectral analysis parameters included 3 maximum allowed missed cleavages, a minimum peptide length of 6. Carbamidomethylation of cysteines was set as a static modification, and 4 maximum variable modifications: methionine oxidation, deamidation of glutamine and asparagine. In addition, three modifications on lysines were included: alkene (C_3H_2O; +54 Da), sulfenic acid ($C_3H_4O_2S$; +104 Da), and thiol (C_3H_2SO; +86 Da) modifications due to remnants of the cross-linker as described in a previous study.[22] For the precursor, mass tolerance was set at 10 ppm, and fragment mass tolerance was set at 20 ppm and 0.5 Da for Orbitrap and ion trap spectra, respectively. A false discovery rate (FDR) was set to 1% using the Percolator algorithm and cross-link peptide spectra matching with the minimum score threshold set at 40.

For our mixed-cross-linking experiments, we limited the search space to ^{14}N-AHA2 due to the computational scaling problem. We then calculated the expected m/z shift for a given cross-link ID by adding the mass value of a single neutron (0.997035 Da) divided by the charge state of the dipeptide being considered, to the m/z of one peptide for every nitrogen atom in each residue (heavy × light cross-link). We repeated this for a case in which the second peptide of the dipeptide was the heavy-labeled one as well. We then used these predicted shifts to identify a matching isotopic envelope for a mixed

https://dx.doi.org/10.1021/acs.biochem.0c00268
Biochemistry 2020, 59, 2210−2225

Table 1. Summary of All Identified C-terminal to N-terminal DSSO Cross-links in AHA2[a]

no.	cross-link	max XlinkX score	no. of CSMs	domain to domain
1	K27 × K888	247.7	10	actuator to C-terminus
2	K27 × K911	214.88	7	actuator to C-terminus
3	K27 × K926	150.27	2	actuator to C-terminus
4	K27 × K934	203.29	1	actuator to C-terminus
5	K53 × K888	184.34	1	actuator to C-terminus
6	K175 × K888	76.72	3	actuator to C-terminus
7	K175 × K897	104.45	3	actuator to C-terminus
8	K175 × K911	60.79	1	actuator to C-terminus
9	K203 × K868	62.69	1	actuator to C-terminus
10	K203 × K888	62.26	1	actuator to C-terminus
11	K203 × K911	59.71	1	actuator to C-terminus
12	K203 × K926	163.16	4	actuator to C-terminus
13	K312 × K863	235.06	18	P-domain to C-terminus
14	K312 × K864	232.34	18	P-domain to C-terminus
15	K312 × K868	209.97	19	P-domain to C-terminus
16	K312 × K888	276.36	23	P-domain to C-terminus
17	K312 × K897	185.51	5	P-domain to C-terminus
18	K312 × K911	256.94	12	P-domain to C-terminus
19	K312 × K926	259.62	10	P-domain to C-terminus
20	K312 × K934	195.8	2	P-domain to C-terminus
21	K338 × K888	204.64	1	N-domain to C-terminus
22	K338 × K911	41.03	1	N-domain to C-terminus
23	K338 × K926	108.75	1	N-domain to C-terminus
24	K386 × K897	140.1	3	N-domain to C-terminus
25	K386 × K911	259.08	5	N-domain to C-terminus
26	K405 × K888	214	5	N-domain to C-terminus
27	K405 × K897	145.71	15	N-domain to C-terminus
28	K405 × K911	280.53	24	N-domain to C-terminus
29	K405 × K926	260.8	7	N-domain to C-terminus
30	K423 × K888	62.26	2	N-domain to C-terminus
31	K423 × K911	186.87	3	N-domain to C-terminus
32	K434 × K911	74.17	1	N-domain to C-terminus
33	K434 × K926	157.38	1	N-domain to C-terminus
34	K441 × K926	134.23	1	N-domain to C-terminus
35	K470 × K897	56.51	1	N-domain to C-terminus
36	K470 × K911	92.76	2	N-domain to C-terminus
37	K519 × K868	222.45	4	P-domain to C-terminus
38	K519 × K888	263.9	28	P-domain to C-terminus
39	K519 × K897	132.09	8	P-domain to C-terminus
40	K519 × K911	236.75	19	P-domain to C-terminus
41	K519 × K926	217.59	5	P-domain to C-terminus
42	K542 × K888	99.57	1	P-domain to C-terminus
43	K580 × K864	60.53	1	P-domain to C-terminus
44	K696 × K868	57.56	2	loop TM6-TM7 to C-terminus
45	K696 × K888	215.15	7	loop TM6-TM7 to C-terminus
46	K696 × K897	175.28	3	loop TM6-TM7 to C-terminus
47	K696 × K911	93.43	3	loop TM6-TM7 to C-terminus
48	K696 × K926	181.87	1	loop TM6-TM7 to C-terminus

[a]No. of CSMs: cross-link spectral matches.

dipeptide. The spectra of cross-links were extracted using FreeStyle (Thermo Fisher Scientific). The mass spectrometry proteomics data were deposited to the ProteomeXchange Consortium via the PRIDE[29] partner repository with the data set identifier PXD018219.

RESULTS

Extensive Cross-Linking between the C-Terminal Domain and Other Domains of AHA2 Suggests Dynamic Interactions Regulate the Catalytic Cycle. In order to identify the sites of interactions between the C-terminal domain and other parts of protein, we purified AHA2 from *Saccharomyces cerevisiae* as described previously[13] and performed DSSO cross-linking at a protein to cross-linker molar ratio of 1:100. The samples were then either subjected to in-solution digestion immediately or were first resolved on SDS-PAGE (Figure S1A). In the latter case, monomer and trimer-sized slices of cross-linked AHA2 were subjected to in-gel digestion before analysis by mass spectrometry. To optimize the fragmentation method for cross-link identification, we tested four different MS methods, as described in a previous study:[28] (i) CID-MS2/ETD-MS2, (ii) CID-MS2/EthCD-MS2, (iii) CID-MS2/HCD-MS2, and (iv) CID-MS2/HCD-MS3. The result (Figure S1B) showed that these fragmentation methods are complementary to each other and the combination of CID and HCD outperforms the other two methods, in agreement with previous studies.[30,31]

It is known that combining different proteases can significantly boost the number of cross-links identified.[28,32] Therefore, to optimize the numbers of detectable AHA2 cross-links, two other enzymes (GluC and chymotrypsin) were used in combination with trypsin for in-solution digestion. The combined identifications resulting from in-solution digestions with these three different proteases increased the total number of identified cross-links for AHA2 to 104 (Figure S1C). Ultimately, the digestion of AHA2 with these three proteases increased the protein's sequence coverage to 85%, including the complete identification of 6 of the ten transmembrane domains of AHA2 (Figure S2). It should be noted that in these methods, only precursor ions with higher charge $>2^+$ were selected for further fragmentation; therefore, the actual coverage of AHA2 using multiple proteases may be higher than this number if including charge 2^+ ions (or even charge 1^+ ions) for MS2 fragmentation, which will be useful in future studies of AHA2 using mass spectrometry.

In total, 142 unique cross-links were identified between different domains of AHA2 (supplementary Table 1). These identifications are combined from the results of both in-solution and in-gel digested samples and were obtained with an Xlink score cutoff threshold of 40, as suggested by a previous study to maximize the confidence in cross-link identifica-

https://dx.doi.org/10.1021/acs.biochem.0c00268
Biochemistry 2020, 59, 2210−2225

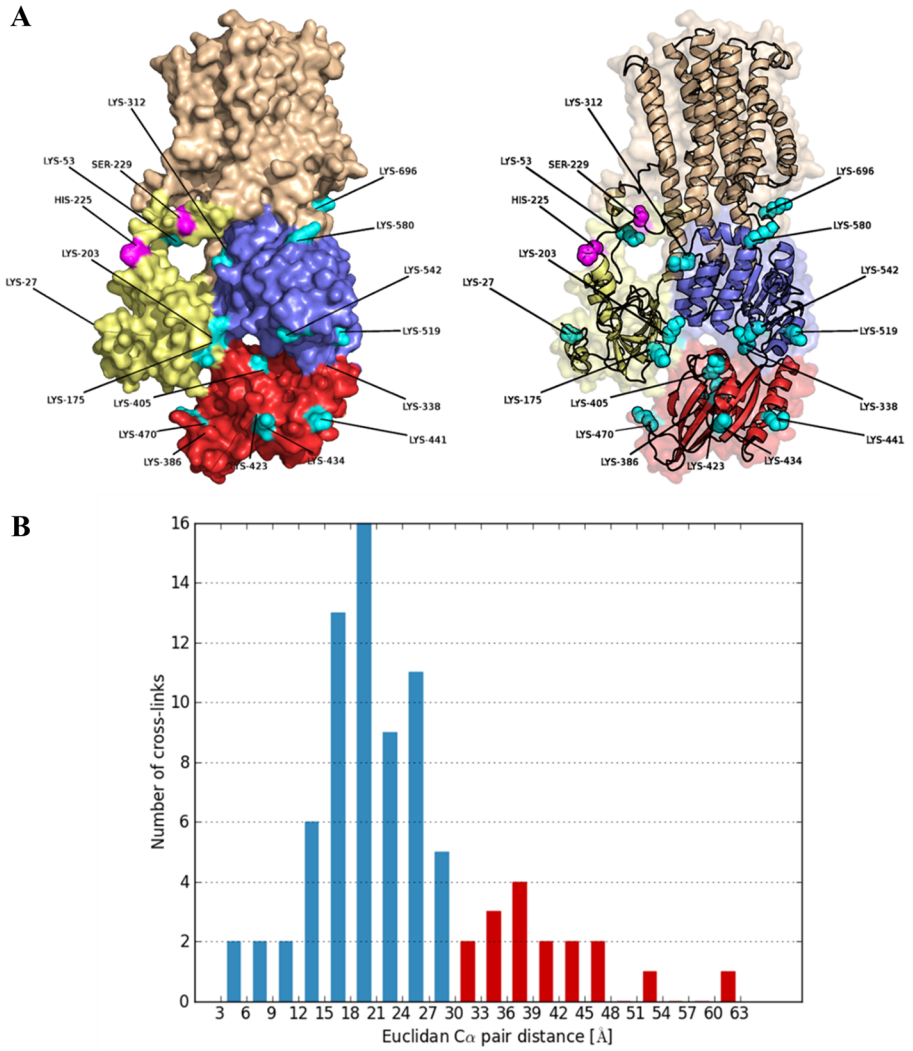

Figure 1. Mapping cross-linked residues to the crystallized structure of monomeric AHA2 (PDB: 5KSD, lacking its C-terminal domain). (A) All of the lysine residues in the nucleotide-binding domain (red), phosphorylation domain (blue), actuator domain (yellow), and transmembrane domain (wheat) that cross-linked to the C-terminal domain are shown in cyan. The purple residues are BPA substitution sites that robustly cross-linked with the C-terminal domain, detected in our earlier study (Nguyen et al., 2018). Left: surface rendering of 5KSD with mapped residues Right: cartoon backbone rendering. (B) Histogram showing the distribution of the AHA2 distance restraints based on the structure of AHA2 lacking the C-terminal domain using Xlink Analyzer and Chimera. Distances ($C_\alpha - C_\alpha$) of less than 30 Å are colored in blue, and distances above 30 Å are colored in red.

tions.[31] Notably, Lys-312 in the phosphorylation domain appeared in 29 cross-links, and Lys-405 in the nucleotide-binding domain appeared in 19 cross-links, suggesting that these are hotspot cross-linking locations. Similarly, at the C-terminal domain, Lys-911 (16 cross-links) and Lys-888 (14 cross-links) are two key residues involved in many different interactions with the rest of the enzyme, indicating that the C-terminal domain's regulatory interactions are highly dynamic.

Among these 142 AHA2-AHA2 cross-links, 48 cross-links formed between the C-terminal domain and other domains of the enzyme (Table 1). All of the residues that cross-linked to the C-terminal domain were mapped to the most current crystal structure of AHA2 (PDB: 5KSD), which lacks the entire C-terminal domain. As shown in Figure 1, the C-terminal domain cross-linked with several lysines in all other domains. For example, 12 cross-links occurred between the C-terminal domain (Lys-868, 888, 897, 911, 926, and 934) and the actuator domain (Lys-27, 53, 175, and 203); 12 cross-links between the C-terminal domain (Lys-888, 897, 911, and 926) and the nucleotide-binding domain (Lys-338, 386, 405, 423, 434, 441, and 470); and 15 cross-links between the C-terminal domain (Lys-863, 864, 868, 888, 897, 911, 926, and 934) and the phosphorylation domain (Lys- 312, 519, 542, and 580). Interestingly, 5 cross-links formed between Lys-696 in the cytoplasmically exposed TM6-TM7 loop and five different lysines in the C-terminal domain (i.e., at K868, K888, K897, K911, and K926) (Figure 2). This might suggest a direct role for the C-terminal domain in mediating proton flux because of the proximity of Lys-696 to the conserved proton binding site Asp-684 (Figure 2A). Interestingly, 37 out of 48 C-terminal cross-links occurred in the first half of the C-terminal domain, involving Lys-863, 864, 868, 888, 897, and 911. Only 11 out of 48 cross-links are involved in the other two sites in the last half of the C-terminal domain, i.e., at Lys-926 and Lys-934. The C-terminal domain also cross-links to itself (supplementary Table 1) including in region II (904−919), which is in agreement with a previous study.[33] These results not only support our previous conclusion that the C-terminal domain may regulate

https://dx.doi.org/10.1021/acs.biochem.0c00268
Biochemistry 2020, 59, 2210−2225

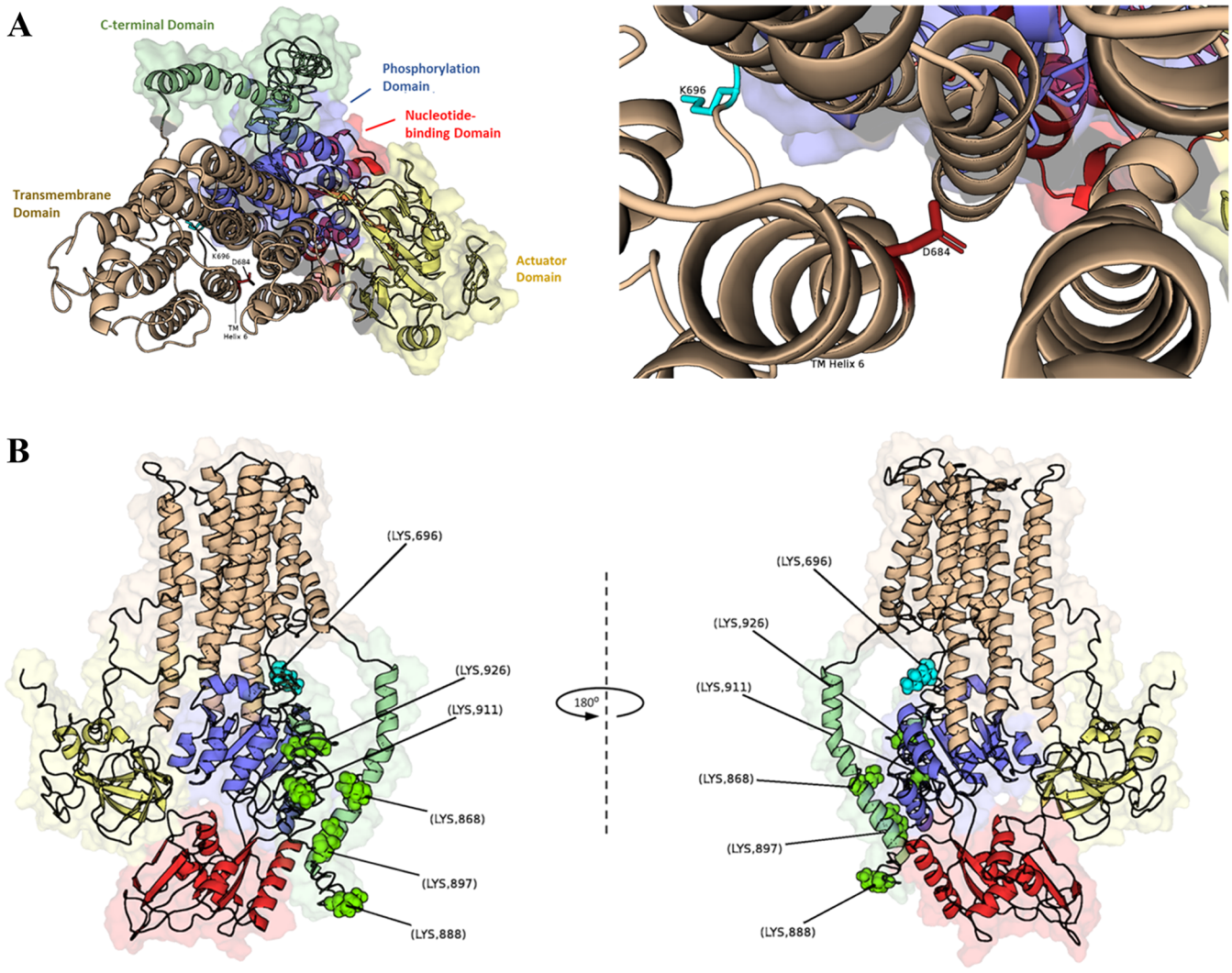

Figure 2. K696 of the cytoplasmic loop between TM6 and TM7 is a novel potential C-terminal domain contact. K696 is located close to the predicted proton binding site (in AHA2, D684), and cross-linking between this position and the C-terminal domain was enriched in the trimeric band. (A) Left: top-down view of the proton binding site in AHA2 through the TM domain. Right: zoomed-in view of TM6 with D684 shown as red sticks; K696 (cyan sticks) is depicted nearby. (B) Contacts on the C-terminal domain that were cross-linked with K696 are indicated as lime spheres.

the enzyme activity by interactions with the actuator domain but also extend the possible inhibitory effect of the C-terminal domain on other domains, directly affecting the phosphorylation/dephosphorylation of the conserved aspartate in the phosphorylation domain as well as the ejection of protons out of the cell.

To visualize the cross-linking result, we mapped all identified cross-links onto the three-dimensional structure of the AHA2 monomer (residues V12 to I844, PDB: 5KSD),[5] allowing measurement of the Euclidean Cα-Cα distance between the residues involved in the cross-link. Distance measurements were performed using Chimera and Xlinkanalyzer.[34,35] 83 out of 142 cross-links identified for AHA2 were able to map onto the structure of AHA2 (except for the region without available structure) shown in Figure 1B and supplementary Table 2. Among these 83 cross-links, 80% of them are within 30 Å, the distance expected for the linker length introduced by amine-to-amine cross-linkers between lysines of a correctly folded protein.[32,36] This suggests that the cross-links reflect the native structure of the AHA2. It is worth noting that this distance measurement does not account for the fact that some of these cross-links may have occurred due to intermolecular interactions between monomers of AHA2.

Interestingly, we also observed cross-linking between the C-terminal domain and other domains in the monomer band of the DSSO-cross-linked AHA2 sample, including K888 with K312; and K911 with K27, K312, K405, and K519 (Supporting Information). An example of cross-linking between K888 and K312 detected in both the monomer and trimer bands is shown in Figure 3A. Notably, cross-links between K312 and K863, K864, K868 were detected only in the trimer band (Figure 3B and Supporting Information), which suggests that these particular cross-links are unique to the oligomeric form of AHA2 similarly to results from our previous interaction studies with the photolabile cross-linker BPA. Figure 3C shows the spectra for the cross-link between K888 and K312 using CID/MS2-HCD/MS3. The top panel shows four signature peaks detected in MS2, and the four lower panels show the MS3 ions from two cross-linked peptides, which were separately fragmented by HCD for peptide identification to maximize coverage of cross-linked peptides. The ability to independently fragment linked

https://dx.doi.org/10.1021/acs.biochem.0c00268
Biochemistry 2020, 59, 2210−2225

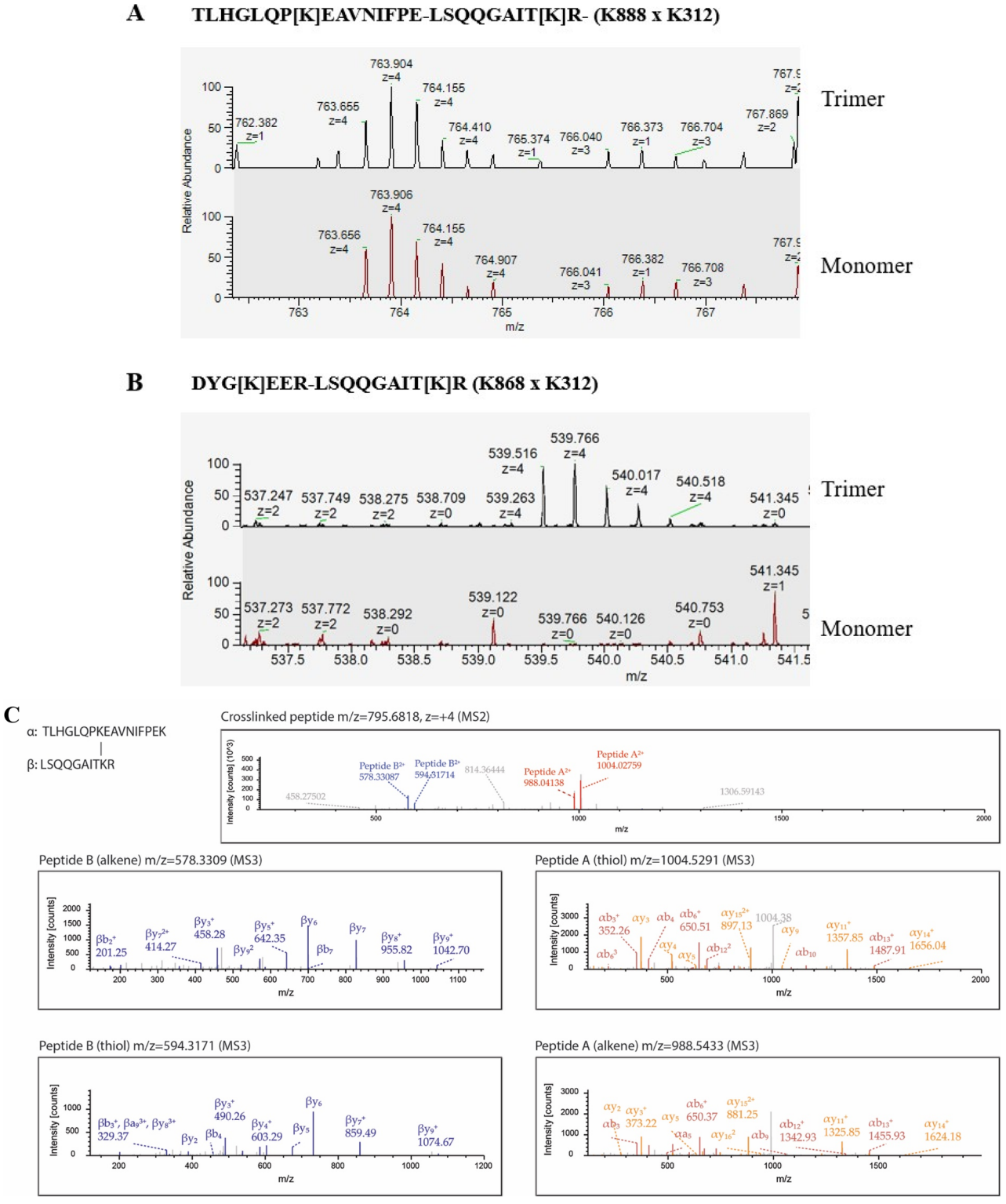

Figure 3. Intramolecular interactions between the N-terminus and the C-terminal domain are distinguishable from intermolecular interactions by their enrichment in separate bands. (A) An example of intramolecular cross-linking, which is detected in both the monomeric and trimeric bands, between K312 of the phosphorylation domain and K888 in the C-terminal domain. (B) An example of a cross-link that was detected exclusively in the trimer band of AHA2, indicating that this cross-link does not arise from an intramolecular interaction. (C) An example of spectra from a cross-link between K888 and K312 identified by the CID-MS2/HCD-MS3 method. Four signature peaks detected in CID-MS2 are shown in the top panel, and the four lower panels show the MS3 acquisition, which was triggered for these linked peptides.

peptides in MS3 is a hallmark advantage that cleavable cross-linkers like DSSO have over noncleavable cross-linkers.

Cross-Linking between Unlabeled AHA2 and ^{15}N-Labeled AHA2 Identifies Novel Intermolecular Interactions of the C-Terminal Domain. To distinguish the intramolecular from intermolecular cross-linking in AHA2 while avoiding the limitations of in-gel digestion, we combined cross-linking with isotopic labeling, which has been used in

https://dx.doi.org/10.1021/acs.biochem.0c00268
Biochemistry 2020, 59, 2210−2225

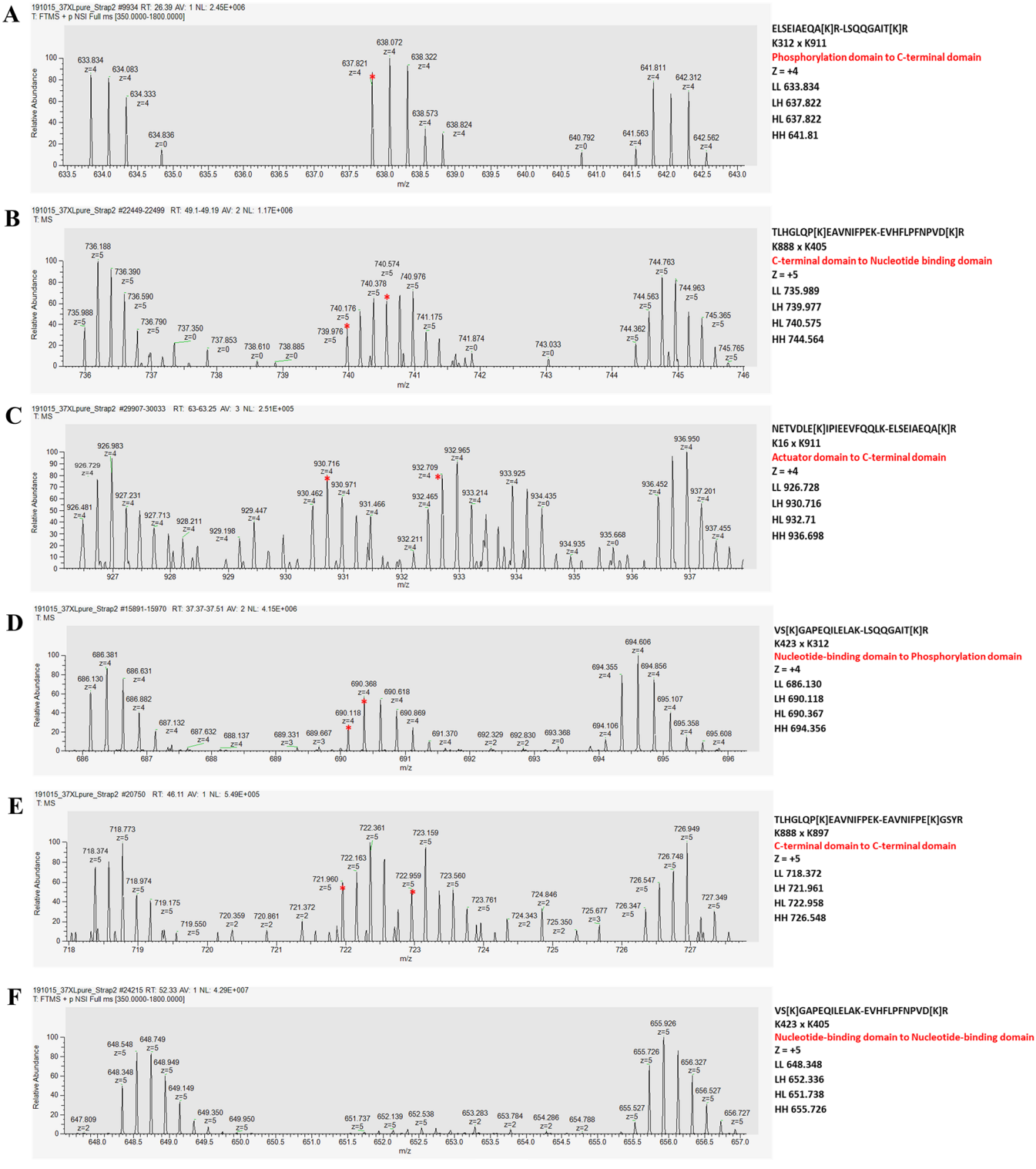

Figure 4. Mixed-isotope cross-links have characteristic spectra with m/z values between those of unlabeled and ^{15}N-labeled peptides. Example spectra for mixed-isotope (intermolecular) DSSO cross-links between separate AHA2 isotopologues are shown for interactions between the C-terminal domain and phosphorylation domain (A), C-terminal domain and nucleotide-binding domain (B), C-terminal domain and actuator domain (C), nucleotide-binding domain and phosphorylation domain (an N-terminal × N-terminal interaction) (D), and finally, between the C-terminal domains of each monomer (E). (F) An example spectrum for an unmixed cross-link ID, which has ^{14}N/^{15}N mixed peaks at the appropriate charge but not at the required minimal abundance of 10%. Red asterisks denote mixed cross-link peaks that match the predicted values (shown to the right of each spectrum) for mixed-isotope-shifted spectra. LL/LH/HL/HH: the calculated single peak m/z values for a cross-link ID with ^{14}N × ^{14}N, ^{14}N × ^{15}N, ^{15}N × ^{14}N, and ^{14}N × ^{15}N composition.

previous studies.[37,38] We generated batches of AHA2 protein that were either labeled with ^{15}N or contained the normal isotopic distribution (only ^{14}N) using a construct that places AHA2 under the control of a galactose inducible promoter;

https://dx.doi.org/10.1021/acs.biochem.0c00268
Biochemistry 2020, 59, 2210−2225

Table 2. Summary of All Identified Crosslink IDs from DSSO Cross-Linking of Heavy (^{15}N) and Unlabeled (^{14}N) AHA2[a]

cross-link	max XlinkXscore	no. of CSMs	domain to domain	mixed?	c-term?
K911 × K312	158.05	3	P-domain to C-terminal domain	yes	yes
K888 × K405	179.67	3	C-terminal domain to N-domain	yes	yes
K926 × K312	308.91	4	C-terminal domain to P-domain	yes	yes
K580 × K598	253.84	3	P-domain to P-domain	no	no
K27 × K911	234.87	2	actuator domain to C-terminal domain	yes	yes
K27 × K49	228.02	3	actuator domain to actuator domain	no	no
K423 × K441	197.13	2	N-domain to N-domain	yes	no
K911 × K868	196.48	1	C-terminal domain to C-terminal domain	yes	yes
K343 × K312	194.06	2	N-domain to P-domain	no	no
K888 × K911	191.13	3	C-terminal domain to C-terminal domain	yes	yes
K355 × K343	187.62	1	N-domain to N-domain	no	no
K405 × K911	187.42	2	N-domain to C-terminal domain	yes	yes
K405 × K312	185.51	3	N-domain to P-domain	yes	no
K449 × K441	181.53	6	N-domain to N-domain	no	no
K338 × K312	179.43	2	N-domain to P-domain	no	no
K386 × K405	177.81	2	N-domain to N-domain	yes	no
K386 × K355	171.38	2	N-domain to N-domain	no	no
K423 × K312	163.83	3	N-domain to P-domain	yes	no
K423 × K449	158.36	2	N-domain to N-domain	yes	no
K598 × K911	158.16	1	P-domain to C-terminal domain	yes	yes
K423 × K405	157.2	12	N-domain to N-domain	no	no
K423 × K911	152.64	2	N-domain to C-terminal domain	yes	yes
K405 × K388	148.22	2	N-domain to N-domain	no	no
K569 × K598	147.29	1	P-domain to P-domain	yes	no
K405 × K441	146.67	4	N-domain to N-domain	no	no
K434 × K405	145	3	N-domain to N-domain	yes	no
K330 × K351	143.46	2	P-domain to N-domain	no	no
K449 × K312	143.24	2	N-domain to P-domain	yes	no
K351 × K312	142.08	3	N-domain to P-domain	no	no
K696 × K312	140.39	2	loop TM6/TM7 to P-domain	yes	no
K519 × K911	138.57	2	P-domain to C-terminal domain	yes	yes
K27 × K405	138.37	2	actuator domain to N-domain	yes	no
K16 × K423	138.33	2	actuator domain to N-domain	yes	no
K49 × K312	136.27	2	actuator domain to P-domain	yes	no
K926 × K897	133.98	1	C-terminal domain to C-terminal domain	yes	yes
K386 × K312	130.1	2	N-domain to P-domain	yes	no
K598 × K312	128.28	2	P-domain to P-domain	yes	no
K190 × K405	126.84	2	actuator domain to N-domain	yes	no
K580 × K312	125.39	1	P-domain to P-domain	yes	no
K16 × K911	122.7	2	actuator domain to C-terminal domain	yes	yes
K696 × K405	122.64	3	loop TM6/TM7 to N-domain	yes	no
K863 × K868	120.3	4	C-terminal domain to C-terminal domain	no	yes
K888 × K897	117.93	2	C-terminal domain to C-terminal domain	yes	yes
K405 × K449	117.7	4	N-domain to N-domain	yes	no
K27 × K423	117.18	2	actuator domain to N-domain	yes	no
K330 × K423	117.18	2	P-domain to N-domain	yes	no
K16 × K405	113.62	1	actuator domain to N-domain	yes	no
K405 × K49	112.42	3	N-domain to actuator domain	yes	no
K190 × K423	112.37	1	actuator domain to N-domain	yes	no
K386 × K423	107.74	2	N-domain to N-domain	yes	no
K897 × K911	107.61	2	C-terminal domain to C-terminal domain	no	yes
K519 × K449	107.5	2	P-domain to N-domain	no	no
K175 × K423	106.52	2	actuator domain to N-domain	yes	no
K926 × K911	103.29	1	C-terminal domain to C-terminal domain	yes	yes
K888 × K868	98.35	3	C-terminal domain to C-terminal domain	no	yes
K27 × K449	98.13	1	actuator domain to N-domain	yes	no
K423 × K49	97.07	2	N-domain to actuator domain	yes	no
K343 × K442	96.34	2	N-domain to N-domain	no	no
K470 × K423	96.19	2	N-domain to N-domain	yes	no
K423 × K338	95.66	1	N-domain to N-domain	no	no
K386 × K49	94.73	2	N-domain to actuator domain	yes	no

https://dx.doi.org/10.1021/acs.biochem.0c00268
Biochemistry 2020, 59, 2210−2225

Table 2. continued

cross-link	max XlinkXscore	no. of CSMs	domain to domain	mixed?	c-term?
K888 × K312	94.19	2	C-terminal domain to P-domain	yes	yes
K519 × K423	93.72	2	P-domain to N-domain	yes	no
K423 × K343	92.93	2	N-domain to N-domain	yes	no
K330 × K312	91.58	2	P-domain to P-domain	no	no
K405 × K343	88.94	1	N-domain to N-domain	yes	no
K434 × K449	88.13	1	N-domain to N-domain	no	no
K897 × K312	86.93	1	C-terminal domain to P-domain	yes	yes
K405 × K442	81.3	2	N-domain to N-domain	yes	no
K405 × K351	81.3	1	N-domain to N-domain	yes	no
K423 × K442	77.92	2	N-domain to N-domain	no	no
K175 × K405	76.9	1	actuator domain to N-domain	yes	no
K897 × K405	75.19	2	C-terminal domain to N-domain	yes	yes
K897 × K868	73.97	1	C-terminal domain to C-terminal domain	no	yes
K386 × K449	73.85	1	N-domain to N-domain	no	no
K519 × K312	73.46	1	P-domain to P-domain	yes	no
K330 × K343	72.17	1	P-domain to N-domain	no	no
K27 × K312	69.43	1	actuator domain to P-domain	yes	no
K449 × K468	68.64	1	N-domain to N-domain	yes	no
K405 × K468	68.64	1	N-domain to N-domain	yes	no
K175 × K386	66.26	1	actuator domain to N-domain	yes	no
K157 × K312	62.72	2	actuator domain to P-domain	no	no
K49 × K57	58.74	3	actuator domain to actuator domain	no	no
K569 × K405	58.08	1	P-domain to N-domain	yes	no
K696 × K423	57.49	1	loop TM6/TM7 to N-domain	yes	no
K696 × K49	57.16	2	loop TM6/TM7 to actuator domain	yes	no
K49 × K911	55.38	1	actuator domain to C-terminal domain	yes	yes
K386 × K343	52.25	1	N-domain to N-domain	no	no
K175 × K598	51.84	1	actuator domain to P-domain	no	no
K434 × K468	50.9	1	N-domain to N-domain	no	no
K386 × K442	49.31	1	N-domain to N-domain	yes	no
K312 × K442	48.12	1	P-domain to N-domain	no	no
K405 × K574	47.81	1	N-domain to P-domain	no	no
K569 × K312	47.26	1	P-domain to P-domain	yes	no
K175 × K49	46.43	1	actuator domain to actuator domain	yes	no
K190 × K312	44.64	1	actuator domain to P-domain	yes	no
K696 × K175	44.62	2	loop TM6/TM7 to actuator domain	no	no
K330 × K405	43.02	1	P-domain to N-domain	no	no
K519 × K468	42.46	1	P-domain to N-domain	no	no
K386 × K434	42.9	1	N-domain to N-domain	yes	no
K175 × K312	41.5	1	actuator domain to phosphorylation	yes	no
K519 × K49	40.99	1	P-domain to actuator domain	yes	no
K27 × K868	40.04	1	actuator domain to C-terminal domain	no	yes

[a]No. of CSMs: number of cross-link spectral matches (CSMs). Mixed?: whether an ID is a $^{14}N/^{15}N$ or $^{15}N/^{14}N$ dipeptide. C-term?: whether a cross-link ID comes from the C-terminal domain.

this construct carries the HIS3 marker and is transformed into the T71 yeast strain lacking the HIS3 gene. After transforming with the plasmid containing AHA2, the T71 yeast becomes autotrophic and can grow in the minimal medium without any amino acid supplements. To express ^{15}N protein and unlabeled (^{14}N) protein, minimal media was prepared containing either ^{15}N ammonium sulfate or ^{14}N ammonium sulfate as the nitrogen source. The colonies were cultured in minimal medium for 5 days with frequent supplements of the fresh medium on each day before harvesting, targeting about 10 mL of cell pellets for each condition. Before mixing two cell populations, three small aliquots of each culture were used to test protein expression levels of AHA2 with Western blot. As shown in Figure S3A, we observed that there is no significant difference in AHA2 expression between culture conditions. We further verified that isotopic labeling had no effect on total protein abundance in our samples. To that end, we mixed cells from each culture (^{14}N and ^{15}N) at a ratio of 1:1 based on the cell density OD_{600} and collected a sample whole-cell extract. We then subjected this to mass spectrometry analysis to confirm that the abundance ratio of protein isotopologues was actually ~1:1 (Figure S3B,C and supplementary Table 3). The isotopic mixture of purified, detergent-solubilized AHA2 from this sample was then incubated in a 37 °C shaker for 30 min and cross-linked with DSSO for one hour at room temperature and analyzed with bottom-up LC−MS. Due to the size of the computational search space from combining mixed-isotope labeling with chemical cross-linking, we limited our search to ^{14}N-AHA2 only. We then calculated the m/z shifts expected for cross-link IDs for possibilities where one of two peptides in

https://dx.doi.org/10.1021/acs.biochem.0c00268
Biochemistry 2020, 59, 2210−2225

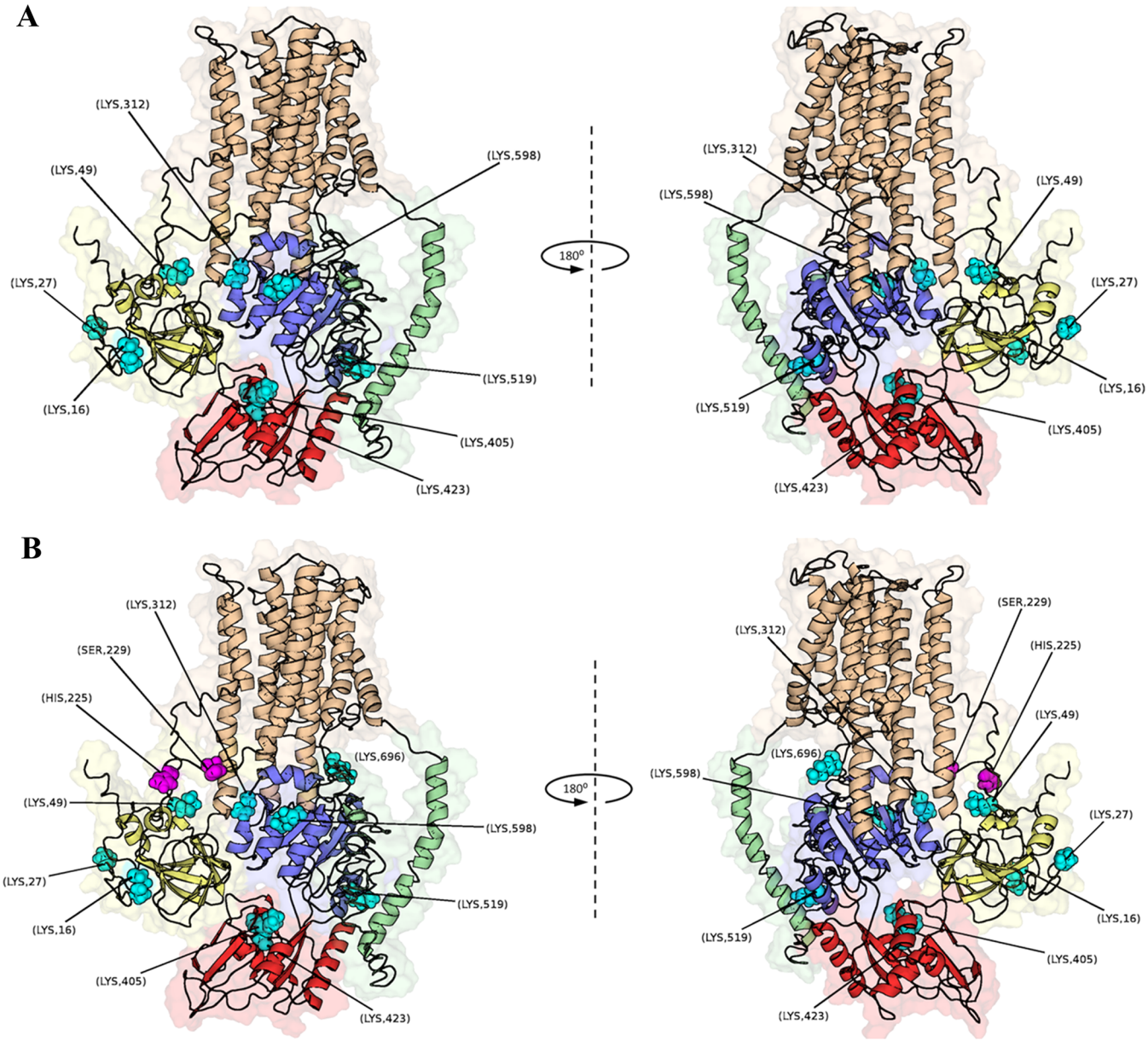

Figure 5. DSSO cross-linking of ^{15}N-labeled AHA2 with ^{14}N-AHA2 indicates new intermolecular interactions between the regulatory C-terminal domain and the other domains of AHA2. (A) ^{14}N−^{15}N and ^{15}N−^{14}N mixed-isotope spectra were detected for 8 lysine positions that reacted with lysines of the C-terminal domain, supplementing the earlier data from site-specific BPA cross-linking. The C-terminal domain density was added to the pre-existing template 5KSD using the protein structure prediction server MODELER. (B) Data in panel A combined with trimer-band-enriched DSSO cross-link IDs (K696) and the BPA cross-linking IDs (magenta spheres, H225B and S229B) identified in our previous study.

the cross-link was fully labeled (^{14}N/^{15}N and ^{15}N/^{14}N) and where both peptides were fully labeled (^{15}N/^{15}N), and used these shifts to manually identify mixed cross-links (Figure 4). A cross-link ID was considered mixed if its spectrum included peaks at our predicted *m/z* values for both ^{14}N/^{15}N and ^{15}N/^{14}N dipeptides in at least a 10% relative abundance of the monoisotopic ^{14}N/^{14}N (or ^{15}N/^{15}N) cross-link IDs (Figure 4A−E); otherwise, we regarded the cross-link ID as unmixed and therefore not likely to be intermolecular (Figure 4F).

In total, we identified 103 unique mixed-isotope cross-links between AHA2 molecules using isotopic labeling. Of these, 68 cross-links had spectra matching our criteria for arising from a mixed cross-link, indicating an intermolecular interaction (Table 2 and Supporting Information). Unsurprisingly, the majority of these unique, intermolecular (mixed) cross-link IDs were confined to the cytoplasmic domains of AHA2; only 4 of these cross-links occurred at one site near the transmembrane domain, the cytoplasmic loop between TM helices 6 and 7. Thirteen of these mixed IDs involved the C-terminal regulatory domain and another region of the protein, suggesting that the C-terminal domain does interact with the neighboring monomer in a "head-to-tail" regulatory fashion. To visualize these intermolecular C-terminal contacts on the protein, we generated a full-length model of AHA2 in the modeling server MODELER[39] using the published structure 5KSD as a template and mapped the cross-linking lysines to it (Figure 5). Considering the number of possible contacts on the C-terminal domain per residue anywhere else in the protein, we concluded that a range of possible configurations of the C-terminal domain can exist during its interactions with

https://dx.doi.org/10.1021/acs.biochem.0c00268
Biochemistry 2020, 59, 2210−2225

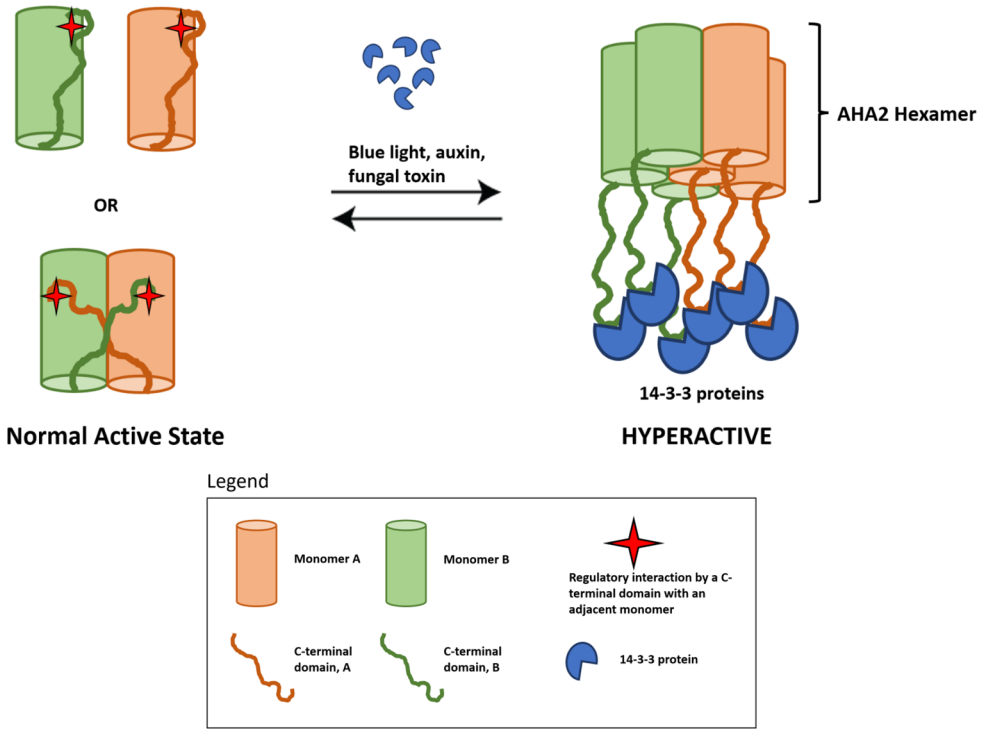

Figure 6. Proposed model for AHA2 regulation. Inside the cell, the PM H^+-ATPase exists as a mixture of monomers and dimers, with the dimer predominating. Both monomers and dimers autoinhibit their enzyme activity through intramolecular interactions and intermolecular interactions between the inhibitory C-terminal domain and other domains (green line or orange line to red star). Under stimulating conditions, three dimers of 14-3-3 associate with three dimers of AHA2 and trap all six C-terminal tails, pulling them away from each monomer and activating the enzyme activity.

a given domain. Notably, K312 of the phosphorylation domain had the most diverse intermolecular interactions with the C-terminal domain (seven in total), suggesting a wide array of possible C-terminal domain/phosphorylation domain configurations and highlighting the importance of inherent flexibility of the C-terminal domain in oligomeric AHA2 (Table 2). This also further supports the possibilities that the C-terminal domain interacts dynamically throughout the catalytic cycle and that the interactions of the environment around K312 are mediated by the oligomeric state of AHA2.

Intermolecular Cross-Linking in the Cytoplasmic Domain Suggests an Interface between Monomers of AHA2. In addition to the C-terminal intermolecular cross-links, we detected numerous intermolecular cross-links between the catalytic domains. Unsurprisingly, the number of unique mixed cross-link IDs that did not involve the C-terminal domain far exceeded the number of C-terminal domain cross-links (~3:1, Table 2). This is consistent with the total surface area of AHA2's other catalytic domains, which is comparatively much larger than that of the C-terminal domain, and likely reflects cytoplasmic-domain/cytoplasmic-domain packing between adjacent AHA2 monomers. Interestingly, the majority of intermolecular cross-links we observed arose from interactions between the nucleotide-binding domains of different AHA2 molecules, suggesting that this domain is important in mediating dimerization. The actuator and phosphorylation domains also showed extensive intermolecular cross-linking, both with each other and with the C-terminal domain. Previously, we identified two actuator domain contacts through site-specific photo-cross-linking of BPA, which was cotranslationally inserted at those sites, with the C-terminus.[13] These new data support and extend this previous work and collectively implicate one or more intermolecular interfaces for AHA2 (Figure 5). However, previous BPA cross-linking data were based on interactions between substituted BPA and any amino acids nearby, whereas DSSO cross-linking relies on interactions that position lysines within cross-linking distance.

Therefore, these DSSO data provide two new pieces of information that can guide future studies on the conformations of AHA2 and its oligomeric state. First, the C-terminal domain is capable of interacting intermolecularly with many regions of AHA2, likely due to its length and flexibility, which are reflected in the many diverse cross-links it was able to form with various domains (Figure S4). Second, the intermolecular cross-links identified through isotope-assisted cross-linking indicate that in an aqueous environment, the solvent-exposed portions of the cytoplasmic domains of separate AHA2 molecules are able to interact sufficiently to cross-link with each other, implying that this protein is able to pack closely in solution. This latter information may not exactly reflect what occurs in the cell, but it does provide information on which regions of AHA2 can reliably make contact with each other between monomers. For intermolecular cross-link IDs identified through our isotope-assisted cross-linking experiments, it is worth noting that among unique N-terminal domain sites that cross-linked with the C-terminal domain, 5 of the 8 C-terminal contacts on the actuator, phosphorylation, and nucleotide-binding domains were previously identified in our earlier DSSO experiments (Figure 5), which validates our methodology but also highlights the ability of isotope-assisted XL-MS to distinguish between interactions that are likely to be intramolecular versus those that arise through intermolecular interactions. The role of the oligomeric interactions of AHA2

https://dx.doi.org/10.1021/acs.biochem.0c00268
Biochemistry 2020, 59, 2210−2225

in regulating catalytic activity merits further investigation, particularly through additional site-specific cross-linking studies *in vivo* to identify the true distance constraints of the physiological interface in the native membrane environment.

DISCUSSION

In this study, we investigated the regulatory interactions of the C-terminal domain of the plasma membrane H^+-ATPase AHA2 using *in vitro* chemical cross-linking with the lysine reactive cross-linker DSSO. We identified eight lysine residues spanning four regions of the C-terminal domain which interact with all other domains (region I, 863, 864, 868; region B, 888 and 897; region II, 911; region C, 926, and 936), suggesting extensive involvement of the C-terminus in different regulatory conformations during the catalytic cycle. Notably, we also observed a C-terminal domain interaction with a cytoplasmic facing loop located between transmembrane domains 6 and 7, suggesting its potential role in the regulation of proton efflux because of the proximity of the C-terminus to the predicted proton binding site (D684) during this interaction. This observation is also consistent with the observation that many activated mutants improved the proton efflux coupling efficiencies of PMA2 and AHA2 in the aforementioned mutagenesis studies.[40,41]

Our chemical cross-linking approach robustly identified novel interactions between the C-terminal domain and all other domains of the enzyme. Combining this cross-linking method of using an MS-cleavable cross-linker with isotopic labeling allowed us to unambiguously study the intermolecular interactions of AHA2. This approach is superior to cross-linking alone and to cross-linking with noncleavable cross-linkers because previous studies employing isotopic labeling and cross-linking with noncleavable cross-linkers reported fewer cross-links than what we obtained with isotopic labeling and DSSO cross-linking.[37,38] We detected numerous mixed-isotope (^{14}N and ^{15}N) cross-links, suggesting this is a powerful technique to study protein oligomerization. With these experiments, we provide new evidence of the intermolecular interactions between the C-terminal domain and other domains on separate molecules of AHA2 (Figure 5 and Table 2), supporting our original "head-to-tail" interaction model (Figure 6). We also detected intramolecular interactions between the C-terminal domain and several residues in the N-terminal domain in AHA2 monomers. This could mean that the C-terminal domain of AHA2 inhibits the enzyme at multiple levels involving both intramolecular and intermolecular interactions with other domains. Interestingly, previous work in our lab has suggested that there are interactions between different isoforms of the H^+-ATPase in *Arabidopsis*.[42] Therefore, future cross-linking studies of the plasma membrane *in planta* may reveal whether the "head-to-tail" regulation between different isoforms of H^+-ATPase in a heterodimeric complex is occurring *in vivo*. It should be noted that the 11 isoforms of AHAs have high protein sequence similarity, which will require careful inspection of data to identify the true heterooligomers between these isoforms. Furthermore, unlike in yeast where AHA2 was heterogeneously expressed to very high levels, a key challenge that must be overcome in structural proteomics of membrane proteins *in planta* is the difficulty of expressing enough of the target protein *in situ* as well. Finally, there is the issue of efficiently delivering the cross-linker to the plasma membrane. Nevertheless, the results from our study provide a useful starting point since they can be used to create a spectral library for targeted mass spectrometry to detect and quantify cross-linked peptides occurring *in planta* under different growth conditions.

In the absence of other monomers, it is important for the cell to regulate AHA2 activity by forming intramolecular interactions with the C-terminal domain. Unfortunately, cross-linking between isotopic homodimers ($^{14}N/^{14}N$ and $^{15}N/^{15}N$) alone is not able to distinguish between intramolecular interactions within the monomer and intermolecular interactions between domains of the homodimer. Therefore, the only way to detect such intramolecular interactions is by first resolving the monomer on the SDS-PAGE gel for in-gel analysis and then subjecting separate gel slices to digestion. However, this method has a much lower digestion efficiency compared to in-solution digestion, limiting coverage, and potentially the detection of certain cross-links. Therefore, future optimization of in-gel digestion methods will be necessary for the analysis of intramolecular cross-links via in-gel digestion.

These results prompted us to update our previous model to account for how the C-terminal domain may regulate enzyme activity by either forming intramolecular interactions with other domains as well as by forming intermolecular interactions when in the oligomeric state (Figure 6). We propose that inside the cell, the plasma membrane H^+-ATPase may exist as monomers, dimers, or other types of oligomers, with the dimeric form being the most abundant.[43] Additionally, it should be noted that this purely oligomeric AHA2 will be different than the hexameric AHA2 complexed with regulatory 14-3-3 protein dimers, which bind to phospho-marks on the C-terminal domain. In such a complex, all C-terminal domains in six monomers are trapped by 14-3-3 protein, causing enzyme activation. Future work using chemical cross-linking on the plasma membrane H^+-ATPase in planta with or without fusicoccin, a fungal toxin that stabilizes the interactions between the C-terminal domain and 14-3-3 protein, would be useful to compare the different arrangements between domains in these different oligomeric states. Answering this question may lead to a better understanding of why the plasma membrane H^+-ATPase appears to exist mainly as dimers inside the cell that only convert into the hexameric form when complexed with 14-3-3 to become highly active.[43] This requirement for 14-3-3 for activation may represent an ATP-saving mechanism the plant uses for when the enzyme does not need to pump protons out of the cell so rapidly. In contrast, under unusual conditions, such as high nutrient availability (like when changing plant cell culture medium to fresh medium), AHA2 is expected to convert from a dimer to a hexamer in complex with six 14-3-3 proteins to enhance the activity of the proton pump. This would be necessary for the uptake of nutrients and for supporting the burst in plant cell growth that would occur in rich medium. In this way, it is more efficient for 14-3-3 to collect all three pairs of AHA2 and then trap six C-terminal domains at once rather than activate each dimer separately; this is a possible explanation for why we never observe other forms of 14-3-3 with AHA2 or observe pure AHA2 hexamers in the plant.[43] The highly dynamic interactions observed between the C-terminal domain and the other domains of AHA2 in these cross-linking experiments raise the exciting possibility that some of these cross-links are occurring in one molecule of AHA2 and reflect multiple snapshots of AHA2 during its catalytic cycle.

https://dx.doi.org/10.1021/acs.biochem.0c00268
Biochemistry 2020, 59, 2210−2225

Alternatively, it is possible that the cross-links can be formed differently within each monomer and between monomers, reflecting monomer−monomer sampling interactions as monomers pack into oligomers in the plasma membrane. Ultimately, a complete understanding of the regulation of this enzyme requires a high-resolution structure of the whole protein including its C-terminus. To this end, chemical cross-linking may help stabilize the C-terminal domain and make it possible to crystallize the full protein for X-ray diffraction. Furthermore, combining chemical cross-linking with cryoEM to investigate the arrangement between domains in the oligomeric AHA2 will elucidate this problem.

An important limitation of DSSO cross-linking is that DSSO has a spacer arm of 10.3 Å that is introduced during cross-linking and bridges the space between cross-linked lysines. This may not reflect a direct interaction between the residues in the native environment and could possibly result from the sufficiently close proximity of the lysines involved in the cross-link. This raises the important caveat that more information is required to distinguish between cross-links that reflect a true biochemical interaction and cross-links that merely form because those lysines are brought into the minimal cross-linking distance by interactions that do not directly involve them. AHA2 has 62 lysine residues, so if we assume that these lysines interact in a random fashion, then there are $62!/(62-2)! \times 2! = 1891$ possible cross-links. In reality, only a small subset of those possible cross-links was observed, suggesting that the limited number of cross-links identified in this experiment is not due to random effect even with the possibility of biologically nonspecific cross-linking. Indeed, most of the lysine residues identified in the C-terminal domain, which cross-linked with other domains, were identified by prior alanine scanning studies as activating mutants and have been independently suggested to directly involved in inhibition of the H^+-ATPase by the C-terminal domain.[7] Therefore, it is plausible that these lysine residues are directly involved in the interaction and regulation of other N-terminal domains and transmembrane domains. Regardless of its limitations, the most important advantage of chemical cross-linking mass spectrometry is that it can unambiguously identify the exact residues involved in the cross-link with high confidence, especially when using the MS-cleavable cross-linker DSSO. This feature led us to the identification of important distance constraints among all domains of AHA2. On average, 40−60 cross-links can be identified for AHA2 in a single DSSO cross-linking experiment, providing a broad look at the whole protein. In contrast, the highly specific cross-linking involved with BPA, which we used in our previous study, limits this work to inspecting one residue at a time.[13] This demonstrates the importance of viewing these two cross-linking approaches as complementary techniques that are best used together. As a best practice in the application, it may be most useful to scan potential candidates using chemical cross-linking, followed by *in vivo* BPA cross-linking informed by the results from chemical cross-linking to search for residue−residue interactions at physiologically relevant distances. In addition, with both technologies, it is important to manipulate the protein's conformation using chemical (e.g., various ligands and pH) and genetic (e.g., site-directed mutants) methods and investigate how this alters the reactivity of the lysines in solution. This data is needed to complement the crystal structure obtained for the protein lacking its C-terminal domain so that an integrated model in which the precise locations of all side chains are known can be derived under the various states of activity that this enzyme is capable of attaining.

■ ASSOCIATED CONTENT

Supporting Information

The Supporting Information is available free of charge at https://pubs.acs.org/doi/10.1021/acs.biochem.0c00268.

Optimization of DSSO cross-link, protein coverage of AHA2, expression of ^{14}N and ^{15}N AHA2, light to heavy peptide abundance ratios, locations of lysine residues forming intermolecular interaction on AHA2 structure (PDF)

Cross-link ID spectra generated from in-gel digestion of monomeric and trimeric AHA2 following cross-linking with DSSO (PDF)

All cross-link ID spectra generated from in-solution digestion of ^{14}N-AHA2 cross-linked with ^{15}N-AHA2 using DSSO ("mixed" cross-links) (PDF)

All cross-link ID positions identified from AHA2 cross-linking with DSSO (XLSX)

Euclidean distances ($C_\alpha - C_\alpha$) between cross-link positions (XLSX)

Values of the log10 abundance ratio (XLSX)

Accession Codes

Uniprot Accession number of AHA2: P19456.

■ AUTHOR INFORMATION

Corresponding Author

Michael R. Sussman − *University of Wisconsin-Madison, Biochemistry Department and the Center for Genome Science Innovation, Madison, Wisconsin 53706, United States*; Phone: (608) 262-8608; Email: msussman@wisc.edu

Authors

Thao T. Nguyen − *University of Wisconsin-Madison, Biochemistry Department and the Center for Genome Science Innovation, Madison, Wisconsin 53706, United States*; orcid.org/0000-0003-3877-3220

Matthew R. Blackburn − *University of Wisconsin-Madison, Biochemistry Department and the Center for Genome Science Innovation, Madison, Wisconsin 53706, United States*

Complete contact information is available at: https://pubs.acs.org/10.1021/acs.biochem.0c00268

Funding

This work was supported mainly by a grant to M.R.S. from DOE (Basic Energy Sciences, DEFG02-88ER13938), together with smaller contributions from a grant to M.R.S. from NSF (MCB-1713899). The stipend for T.T.N. was also provided by graduate fellowships from the Department of Biochemistry, University of Wisconsin-Madison. M.R.B. was supported by NSF (MCB-1943816), the Morgridge Foundation, the Sam C. Smith Graduate Fellowship in Biochemistry, and a Biochemistry Teaching Fellowship from the Department of Biochemistry, University of Wisconsin-Madison.

Notes

The authors declare no competing financial interest.

■ ACKNOWLEDGMENTS

We would like to thank Brian J. Conti for LC-MS/MS assistance and helpful discussions, Brenda Schilke (Craig lab at

UW Madison) for sharing the T71 yeast strain, and all other Sussman's lab members for their support.

REFERENCES

(1) Morsomme, P., and Boutry, M. (2000) The plant plasma membrane H^+-ATPase: structure, function and regulation. *Biochim. Biophys. Acta, Biomembr. 1465*, 1−16.
(2) Palmgren, M. G. (2001) PLANT PLASMA MEMBRANE H^+-ATPases: Powerhouses for Nutrient Uptake. *Annu. Rev. Plant Physiol. Plant Mol. Biol. 52*, 817−845.
(3) Haruta, M., Gray, W. M., and Sussman, M. R. (2015) Regulation of the plasma membrane proton pump (H^+-ATPase) by phosphorylation. *Curr. Opin. Plant Biol. 28*, 68−75.
(4) Duby, G., Poreba, W., Piotrowiak, D., Bobik, K., Derua, R., Waelkens, E., and Boutry, M. (2009) Activation of plant plasma membrane H^+-ATPase by 14−3-3 proteins is negatively controlled by two phosphorylation sites within the H^+-ATPase C-terminal region. *J. Biol. Chem. 284*, 4213−4221.
(5) Pedersen, B.ør. P., Buch-Pedersen, M. J., Preben Morth, J., Palmgren, M. G., and Nissen, P. (2007) Crystal structure of the plasma membrane proton pump. *Nature 450*, 1111−1114.
(6) Falhof, J., Pedersen, J. T., Fuglsang, A. T., and Palmgren, M. (2016) Plasma Membrane H^+-ATPase Regulation in the Center of Plant Physiology. *Mol. Plant 9*, 323−337.
(7) Axelsen, K. B., Venema, K., Jahn, T., Baunsgaard, L., and Palmgren, M. G. (1999) Molecular dissection of the C-terminal regulatory domain of the plant plasma membrane H^+-ATPase AHA2: Mapping of residues that when altered give rise to an activated enzyme. *Biochemistry 38*, 7227−7234.
(8) Palmgren, M. G., Larsson, C., and Sommarin, M. (1990) Proteolytic activation of the plant plasma membrane H^+-ATPase by removal of a terminal segment. *J. Biol. Chem. 265*, 13423−13426.
(9) Palmgren, M. G., Sommarin, M., Serrano, R., and Larsson, C. (1991) Identification of an autoinhibitory domain in the C-terminal region of the plant plasma membrane H^+-ATPase. *J. Biol. Chem. 266*, 20470−20475.
(10) Regenberg, B., Villalba, J. M., Lanfermeijer, F. C., and Palmgren, M. G. (1995) C-terminal deletion analysis of plant plasma membrane H^+-ATPase: yeast as a model system for solute transport across the plant plasma membrane. *Plant Cell 7*, 1655−1666.
(11) Wielandt, A. G., Pedersen, J. T., Falhof, J., Kemmer, G. C., Lund, A., Ekberg, K., Fuglsang, A. T., Pomorski, T. G., Buch-Pedersen, M. J., and Palmgren, M. (2015) Specific Activation of the Plant P-type Plasma Membrane H^+-ATPase by Lysophospholipids Depends on the Autoinhibitory N- and C-terminal Domains. *J. Biol. Chem. 290*, 16281−16291.
(12) Pedersen, J. T., Falhof, J., Ekberg, K., Buch-Pedersen, M. J., and Palmgren, M. (2015) Metal Fluoride Inhibition of a P-type H^+ Pump Stabilization of the Phosphoenzyme Intermediate Contributes to Post-translational Pump Activation. *J. Biol. Chem. 290*, 20396−20406.
(13) Nguyen, T. T., Sabat, G., and Sussman, M. R. (2018) In vivo cross-linking supports a head-to-tail mechanism for regulation of the plant plasma membrane P-type H^+-ATPase. *J. Biol. Chem. 293*, 17095−17106.
(14) Leitner, A., Walzthoeni, T., Kahraman, A., Herzog, F., Rinner, O., Beck, M., and Aebersold, R. (2010) Probing native protein structures by chemical cross-linking, mass spectrometry, and bioinformatics. *Mol. Cell. Proteomics 9*, 1634−1649.
(15) Rappsilber, J. (2011) The beginning of a beautiful friendship: cross-linking/mass spectrometry and modelling of proteins and multi-protein complexes. *J. Struct. Biol. 173*, 530−540.
(16) Leitner, A., Faini, M., Stengel, F., and Aebersold, R. (2016) Crosslinking and Mass Spectrometry: An Integrated Technology to Understand the Structure and Function of Molecular Machines. *Trends Biochem. Sci. 41*, 20−32.
(17) Schneider, M., Belsom, A., and Rappsilber, J. (2018) Protein Tertiary Structure by Crosslinking/Mass Spectrometry. *Trends Biochem. Sci. 43*, 157−169.
(18) O'Reilly, F. J., and Rappsilber, J. (2018) Cross-linking mass spectrometry: methods and applications in structural, molecular and systems biology. *Nat. Struct. Mol. Biol. 25*, 1000−1008.
(19) Chen, Z. A., and Rappsilber, J. (2018) Protein Dynamics in Solution by Quantitative Crosslinking/Mass Spectrometry. *Trends Biochem. Sci. 43*, 908−920.
(20) Schmidt, C., and Robinson, C. V. (2014) A comparative cross-linking strategy to probe conformational changes in protein complexes. *Nat. Protoc. 9*, 2224−2236.
(21) Yu, C., Huszagh, A., Viner, R., Novitsky, E. J., Rychnovsky, S. D., and Huang, L. (2016) Developing a Multiplexed Quantitative Cross-Linking Mass Spectrometry Platform for Comparative Structural Analysis of Protein Complexes. *Anal. Chem. 88*, 10301−10308.
(22) Kao, A., Chiu, C. L., Vellucci, D., Yang, Y., Patel, V. R., Guan, S., Randall, A., Baldi, P., Rychnovsky, S. D., and Huang, L. (2011) Development of a novel cross-linking strategy for fast and accurate identification of cross-linked peptides of protein complexes. *Mol. Cell. Proteomics 10*, M110.002212.
(23) Liu, F., Lossl, P., Scheltema, R., Viner, R., and Heck, A. J. R. (2017) Optimized fragmentation schemes and data analysis strategies for proteome-wide cross-link identification. *Nat. Commun. 8*, 15473.
(24) Liu, F., Rijkers, D. T., Post, H., and Heck, A. J. (2015) Proteome-wide profiling of protein assemblies by cross-linking mass spectrometry. *Nat. Methods 12*, 1179−1184.
(25) Liu, F., Lossl, P., Rabbitts, B. M., Balaban, R. S., and Heck, A. J. R. (2018) The interactome of intact mitochondria by cross-linking mass spectrometry provides evidence for coexisting respiratory supercomplexes. *Mol. Cell. Proteomics 17*, 216−232.
(26) Zougman, A., Selby, P. J., and Banks, R. E. (2014) Suspension trapping (STrap) sample preparation method for bottom-up proteomics analysis. *Proteomics 14*, 1006−1000.
(27) Crowell, A. M., Wall, M. J., and Doucette, A. A. (2013) Maximizing recovery of water-soluble proteins through acetone precipitation. *Anal. Chim. Acta 796*, 48−54.
(28) Ser, Z., Cifani, P., and Kentsis, A. (2019) Optimized Cross-Linking Mass Spectrometry for in Situ Interaction Proteomics. *J. Proteome Res. 18*, 2545−2558.
(29) Perez-Riverol, Y., Csordas, A., Bai, J., Bernal-Llinares, M., Hewapathirana, S., Kundu, D. J., Inuganti, A., Griss, J., Mayer, G., Eisenacher, M., Perez, E., Uszkoreit, J., Pfeuffer, J., Sachsenberg, T., Yilmaz, S., Tiwary, S., Cox, J., Audain, E., Walzer, M., Jarnuczak, A. F., Ternent, T., Brazma, A., and Vizcaino, J. A. (2019) The PRIDE database and related tools and resources in 2019: improving support for quantification data. *Nucleic Acids Res. 47*, D442−D450.
(30) Smith, D. L., Gotze, M., Bartolec, T. K., Hart-Smith, G., and Wilkins, M. R. (2018) Characterization of the Interaction between Arginine Methyltransferase Hmt1 and Its Substrate Npl3: Use of Multiple Cross-Linkers, Mass Spectrometric Approaches, and Software Platforms. *Anal. Chem. 90*, 9101−9108.
(31) Stieger, C. E., Doppler, P., and Mechtler, K. (2019) Optimized Fragmentation Improves the Identification of Peptides Cross-Linked by MS-Cleavable Reagents. *J. Proteome Res. 18*, 1363−1370.
(32) Leitner, A., Reischl, R., Walzthoeni, T., Herzog, F., Bohn, S., Forster, F., and Aebersold, R. (2012) Expanding the chemical cross-linking toolbox by the use of multiple proteases and enrichment by size exclusion chromatography. *Mol. Cell. Proteomics 11*, M111.014126.
(33) Ottmann, C., Marco, S., Jaspert, N., Marcon, C., Schauer, N., Weyand, M., Vandermeeren, C., Duby, G., Boutry, M., Wittinghofer, A., Rigaud, J. L., and Oecking, C. (2007) Structure of a 14−3-3 coordinated hexamer of the plant plasma membrane H^+-ATPase by combining X-ray crystallography and electron cryomicroscopy. *Mol. Cell 25*, 427−440.
(34) Kosinski, J., von Appen, A., Ori, A., Karius, K., Muller, C. W., and Beck, M. (2015) Xlink Analyzer: software for analysis and visualization of cross-linking data in the context of three-dimensional structures. *J. Struct. Biol. 189*, 177−183.
(35) Pettersen, E. F., Goddard, T. D., Huang, C. C., Couch, G. S., Greenblatt, D. M., Meng, E. C., and Ferrin, T. E. (2004) UCSF

https://dx.doi.org/10.1021/acs.biochem.0c00268
Biochemistry 2020, 59, 2210−2225

chimera - A visualization system for exploratory research and analysis. *J. Comput. Chem. 25*, 1605−1612.
(36) Merkley, E. D., Rysavy, S., Kahraman, A., Hafen, R. P., Daggett, V., and Adkins, J. N. (2014) Distance restraints from cross-linking mass spectrometry: mining a molecular dynamics simulation database to evaluate lysine-lysine distances. *Protein Sci. 23*, 747−759.
(37) Pettelkau, J., Thondorf, I., Theisgen, S., Lilie, H., Schroder, T., Arlt, C., Ihling, C. H., and Sinz, A. (2013) Structural analysis of guanylyl cyclase-activating protein-2 (GCAP-2) homodimer by stable isotope-labeling, chemical cross-linking, and mass spectrometry. *J. Am. Soc. Mass Spectrom. 24*, 1969−1979.
(38) Zybailov, B., Gokulan, K., and Wiese, J. (2015) Analysis of Protein-protein Interaction Interface between Yeast Mitochondrial Proteins Rim1 and Pif1 Using Chemical Cross-linking Mass Spectrometry. *J. Proteomics Bioinf. 8*, 243−252.
(39) Sali, A., and Blundell, T. L. (1993) Comparative protein modelling by satisfaction of spatial restraints. *J. Mol. Biol. 234*, 779−815.
(40) Baunsgaard, L., Venema, K., Axelsen, K. B., Villalba, J. M., Welling, A., Wollenweber, B., and Palmgren, M. G. (1996) Modified plant plasma membrane H^+-ATPase with improved transport coupling efficiency identified by mutant selection in yeast. *Plant J. 10*, 451−458.
(41) Morsomme, P., dExaerde, A. D., DeMeester, S., Thines, D., Goffeau, A., and Boutry, M. (1996) Single point mutations in various domains of a plant plasma membrane H^+-ATPase expressed in Saccharomyces cerevisiae increase H^+-pumping and permit yeast growth at low pH. *EMBO J. 15*, 5513−5526.
(42) Rodrigues, R. B., Sabat, G., Minkoff, B. B., Burch, H. L., Nguyen, T. T., and Sussman, M. R. (2014) Expression of a translationally fused TAP-tagged plasma membrane proton pump in Arabidopsis thaliana. *Biochemistry 53*, 566−578.
(43) Kanczewska, J., Marco, S., Vandermeeren, C., Maudoux, O., Rigaud, J. L., and Boutry, M. (2005) Activation of the plant plasma membrane H^+-ATPase by phosphorylation and binding of 14−3-3 proteins converts a dimer into a hexamer. *Proc. Natl. Acad. Sci. U. S. A. 102*, 11675−11680.

https://dx.doi.org/10.1021/acs.biochem.0c00268
Biochemistry 2020, 59, 2210−2225